Traveling cortical netwave

Ernst Rudolf M. Hülsmann[1]

ABSTRACT

The brain creates a physical response out of signals in a cascade of streaming transformations. These transformations occur over networks, which have been described in anatomical, cyto-, myeloarchitectonic and functional research. The totality of these networks was modelled and synthesised in phases across a continuous time-space-function axis, through ascending and descending hierarchical levels of association via traveling netwaves, where localised disorders might spread locally throughout the neighbouring tissues.

This study quantified this model empirically with time-resolving functional magnetic resonance imaging of an imperative, visually-triggered, self-delayed, therefor double-event related response task. The resulting time series unfold in the range of slow cortical potentials the temporal integrity of a cortical pathway from the source of perception to the mouth of reaction in and out of known functional, anatomical and cytoarchitectonic networks. These pathways are consolidated in phase images described by a small vector matrix, which leads to massive simplification of causal and connectivity modelling and even to simple technical applications.

INTRODUCTION

On a first sight it seems to be self-evident that a local perturbation within the cortical sheet should spread locally. The underpinning networks (tab. I), dictating the pathway from the start to the end, have been developed using different technologies and have varying numbers of nodes: anatomical[7-14,39] cards are produced, underpinned by fasciculi and smaller subcortical connectomes[23-27] and structured using cytoarchitectonic[15-22] atlases. These biological networks carry functions which, originally descriptively[28-30] defined, lead, with increasing relational formalisation, to the low-dimensional multifocal cards from dynamic functional magnetic imaging (dfMRI) seen in resting states[40-65].

The networks are subject to a vectored dynamic system: in its multiple primary areas influxes of information flow inside and intermingle before running towards the only outlet in the primary motor area. This produces well defined temporal, spatial and functional boundary conditions. The system, even taking into account systemic feedforward-feedback-loops, yields a linear function and thus, using Hebbian[1] principles as a basis, Mesulam[2,3,4] develops a model (fig. I) where an equally linear thought stream is represented via four levels of association. Across the four levels, a temporal, spatial and functional hierarchical axis, a unique vector is created, displaying a predisposition for certain spatial directions. This four-dimensional phase space illustrates not only effective but also causal and structural connectivity by using orthogonal, inter- and intra-associative projections:

The cycling phase might be started with the perception of a stimulus in a primary, idiotypical, unimodal association area, as e.g. within the visual cortex (ai); discrimination occurs further upstream in a secondary, still modality-specific association area (aii); heteromodal and often conscious integration follows in a tertiary, high-order association area (aiii); and as highest association area, a limbic, emotional response will upspring (l). Further ahead in time, the chain of ai-aii-aiii in reverse, falls down in descending order via a tertiary multimodal level of association, as in prefrontal thought processes (aiii); the anticipatory planning of movements, as in the vast secondary monomodal, supplementary-motor area (aii); to the execution of the movement in the primary level of association (ai), the motor cortex – a process of execution which ultimately triggers the ai-aii-aiii chain once again: this time through self-perception which takes place in the primary somatosensory area (ai) over unimodal discrimination in Brodmannarea 5 (aii) to multimodal parietal regions (aiii), resulting in temporal models as shown in table II.

Independent of complex, dispersed processes, the order of the sequence ai-aii-aiii-l-aiii-aii-ai should be retained like a palindrome as a quasi-periodic pattern and be continually, sequentially repeated in parallel and with varying phase lengths, just as the perception-reaction sequence involved in all systematic thought processes also remains chronological and recurs rapidly throughout the day and gradually over the course of a lifetime in an ever-repeating self-similar loop.

The model raises a series of prognoses regarding the where, what and when of a transformation whose content is ultimately arbitrary and of the likelihood of such a linear, successive combination occurring. Regulated by

[1] Heinrich Uebersee Institut. 26 Rue de Bonn. Postfach 112. CH-3186 Guin. Switzerland. ernesthuelsmann@gmail.com

Object	Author	Brain coverage/nodes				
		Wohle brain	Cerebral cortex	Cerebellum	Subcortical	networks
Space	Talairach Tournoux 1957	x				
	Maziotta 1995	x				
Macroanatomy	Ecker 1869		x			
	Smith 1907		x			
	AAL Atlas 2002	116	83	23	10	
	Makris 2006	69				
	Desikan 2006		70			
	Gousias 2008		83			
	Destrieux Atlas 2010		74			
	Mindboggle Klein 2012		50			
	MarsAtlas Auzias 2016	x	41	7		
Cytoarchitecture	Campbell 1905		12			
	Brodmann 1909		49			
	von Economo 1925		107			
	Sarkisov 1949		64			
	Bailey 1951		4			
	Lacadie 2008		55			
	JuBrain Eickhoff 2005		100			
Myeloarchitecture	Vogt 1919			x		
	Flechsig 1897 1920					5
	Geschwind 1965		102		6	36
	Catani 2005					5
	Van Essen 2012		x	x	x	
Function descriptive	Gall 1791		33			
	Zilles 1994		49			13
	Van Essen 1998		49			7
	Mesulam 2000		12			4

Object	Author	Brain coverage/nodes				
		Wohle brain	Cerebral cortex	Cerebellum	Subcortical	networks
Function visual	Van Essen 1992		38			12
	Ungerleider 1995		36			6
	Glerean 2012		3			
	Naser 2017		9			
	Grandinetti 3013		12			
	Pitzalis 2015		11			
	Yeo 2011		6			5
Function motoric	Zilles 1995		7(9)			
Function rsfMRI	Smith 2009		18			10
	Andrews-Hanna 2010		11			3
	Bellec 2010	7-444				
	Power 2011	x				14
	Choi 2012		17	x	x	7,17
	Craddock 2012	10 - 1000				
	Shen 2013	93,184,278				
	Spreng 2013		43			3
	Wang 2015		x	x		18
	AICHA Joliot 2015		122/50	20		
	Zhang 2015		15			9
	Fan 2016			x		
	Gordon 2016		333			
	Braga 2017					3
	Schaefer 2018		100-1000			
	Kong 2018		x			17
Other	Huth 2016		160			
	Fan 2016		123		x	
	Glasser 2016		180			
	Varikuti 2018	2-500				

Table I. Nodes and networks in parcellations of the human brain.
The space, the anatomy, the cytoarchitecture, the myeloarchitecture and the functions supported by the aforementioned structures, for the whole cortex as well as for the visual and motoric subsystems. Given are the nodes (per hemisphere) and, if investigated, their organization in networks and hierarchies.
Space – constituent Talairach[5] and MNI[6] spaces.
Macroanatomy - Different anatomical subdivisions, as per old observations such as Ecker[7], Smith[8] and newer ones as Tzourio-Mazoyer & al.[9], Harvard–Oxford Atlas Makris & al.[10], Desikan–Killiany Atlas Desikan & al.[11], Hammersmith Atlas Gousias & al.[39], Destrieux & al.[12], Klein & al.[13], Auzias & al.[14].
Cytoarchitecture – Campbell[15], Brodmann[16] and its transcription by the Yale Bioimage Suite Package Lacardie & al.[17], von Economo & Koskinas[18], Sarkisov & Filimonoff[19], Bailey & von Bonin[20], Eickhoff & al.[21,22] Torso.
Myeloarchitecture - as per Vogt & Vogt[23] , Flechsig[24], Geschwind[25], Catani & Ffytch[26] and the ongoing efforts of the Human-Connectome-Project[27] on cortical parcelling.
Function descriptive – Gall[28] , Zilles & Rehkaemper[29], Van Essen & al.[30], the two latter ones consolidating Brodmanns atlas.
Function visual – Van Essen & al.[31] (12 hierarchies), Ungerleider[32] (6 hierarchies), Glerean & al.[33] (dynamic regional phase synchrony), Naser & al.[34], Grandinetti & al.[35], Pitzalis & al.[36], Yeo & al.[37].
Function motoric - Zilles & al.[38] (integrating architectonic, transmitter receptor, MRI and PET data).
Function rsfMRI – resting state functional magnetic resonance imaging observing networks (default mode network (consisting of a core, a dorsal medial and a medial temporal subsystem), executive control network, frontoparietal network, dorsal and ventral attention network, salience network, several visual and sensorimotor networks):[39]Smith & al.[40] (ICA, 7000 subjects), Andrews-Hanna & al.[41,42] (hierarchical relations within the default network), Bellec & al.[43], Power & al.[44], Yeo & al.[38] (clustering ICA, 1000 subjects, separation of the early sensory and late motor cortices), Buckner & al.[45,46] (seedbased ICA), Choi & al.[47,48] (caudal-rostral parietal and rostro-caudal frontal hierarchies), Craddock & al.[49] (spectral clustering), Shen & al.[50], Spreng & al.[51] (hierarchical relations between three networks, see table II), Wang & al.[52] (interindividual), Joliot & al.[53], Zhang & al.[54] (directionality, subdividing two visual networks), Fan & al.[55] (eigenentropy), Gordon & al.[56] (individual), Braga & al.[57] (within individual), Schaefer & al.[58] (clustering and local boundary detection), Kong & al.[59] (individual, character-predictive),
Other – Huth & al.[60,61] (language), Fan & al.[62] (multimodal, structure, connectivity, function), Glasser & al.[63] (multimodal), Varikuti & al.[64].
See Eickhoff & al.[65] for a detailed discussion.

While the descriptive function defines output variables by psychological terms (such as thoughts, memories, feelings and mechanical actions, optical or acoustic perception), dfMR-imaging determines the functions as mathematical relations between regions. As a result, one region may yield speed in relation to another region, but a completely different variable in relation to a third region.

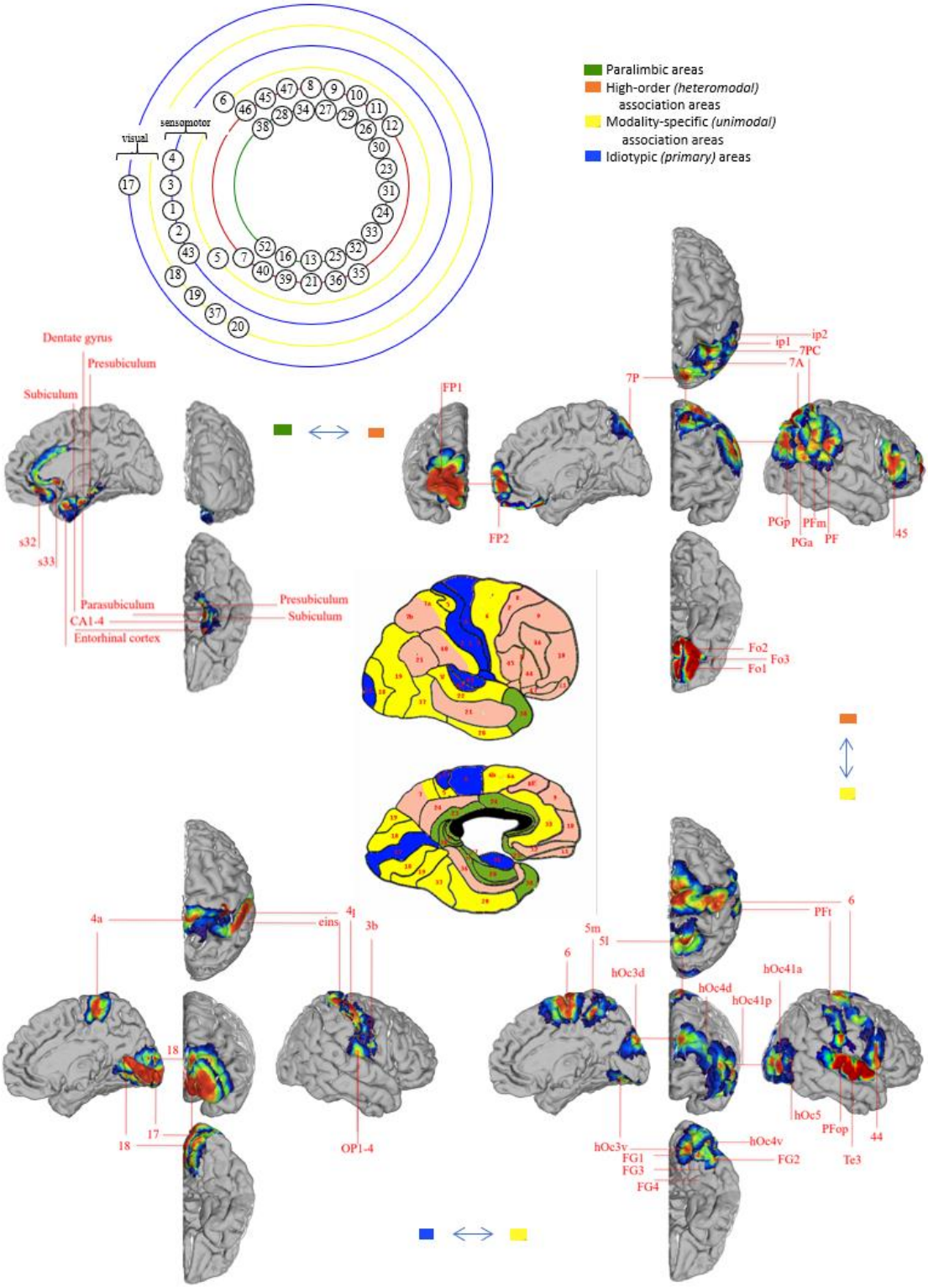

Figure I. Traveling netwaves in Mesulam's[2,3] phase-hierarchy model of Brodmann areas.
Above - The phase space shows Brodmann areas (numbers in circles) for two primary (visual and sensorimotor) and the consecutive secondary, tertiary and limbic areas, corresponding 2π to the margin from perception to perception. The colours of the hierarchical rings correspond to Mesulam's key (right). During a visuo-motor task, the phase repetition means that both unimodal somatosensory hierarchies rings first follow 2π on both unimodal visual rings.

Below - Temporal and spatial hierarchies in Mesulam's anatomical/histological/functional model (centre, adapted from Mesulam[3]) translate to the cytoarchitectures published in JuBrain[66] (sup. mov. I).

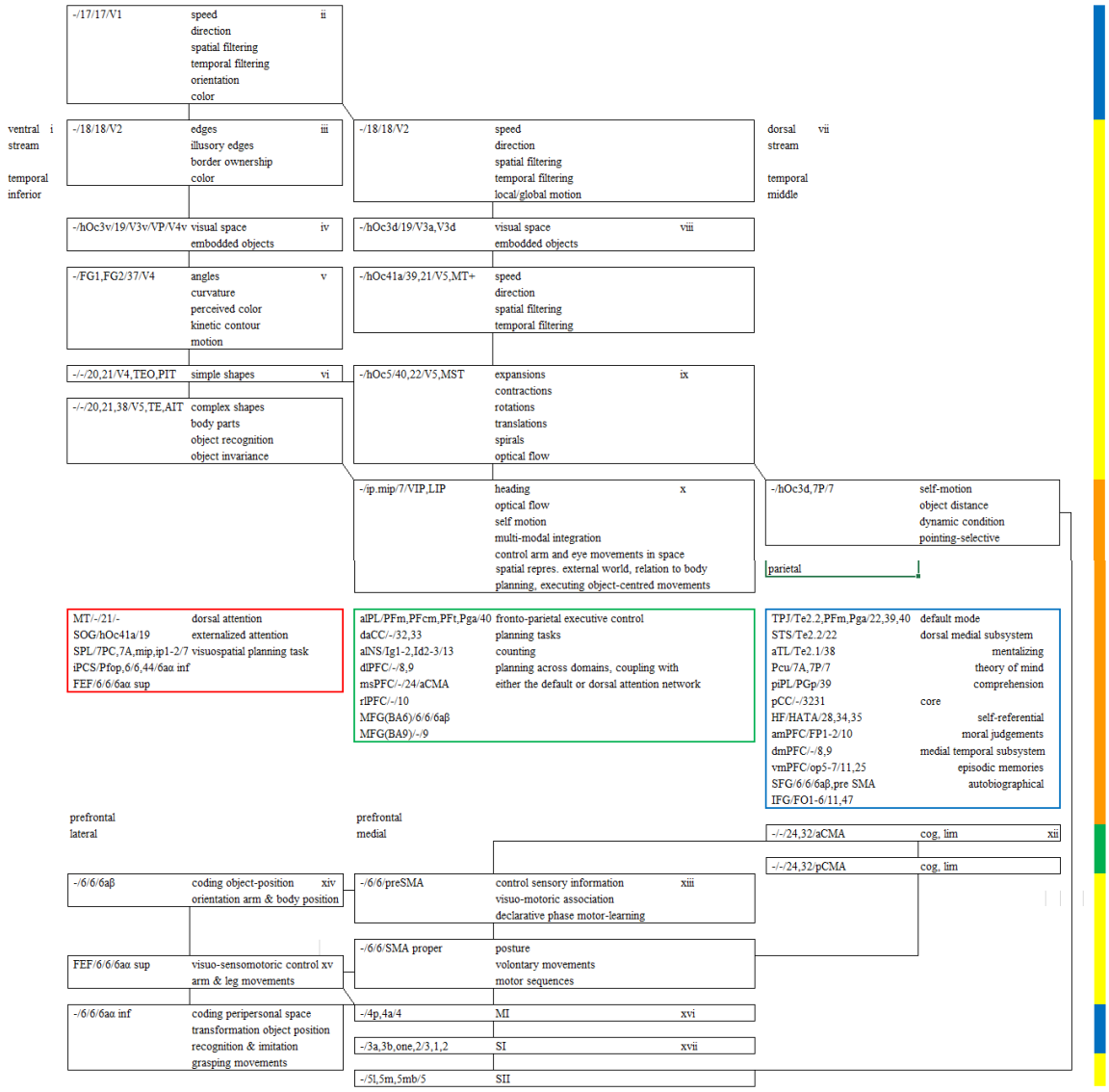
-/17/17/V1
speed
direction
spatial filtering
temporal filtering
orientation
color
ii
ventral stream
temporal inferior
i
-/18/18/V2
edges
illusory edges
border ownership
color
iii
-/18/18/V2
speed
direction
spatial filtering
temporal filtering
local/global motion
dorsal stream
temporal middle
vii
-/hOc3v/19/V3v/VP/V4v
visual space
embodded objects
iv
-/hOc3d/19/V3a,V3d
visual space
embodded objects
viii
-/FG1,FG2/37/V4
angles
curvature
perceived color
kinetic contour
motion
v
-/hOc41a/39,21/V5,MT+
speed
direction
spatial filtering
temporal filtering
-/-/20,21/V4,TEO,PIT
simple shapes
vi
-/-/20,21,38/V5,TE,AIT
complex shapes
body parts
object recognition
object invariance
-/hOc5/40,22/V5,MST
expansions
contractions
rotations
translations
spirals
optical flow
ix
-/ip.mip/7/VIP,LIP
heading
optical flow
self motion
multi-modal integration
control arm and eye movements in space
spatial repres. external world, relation to body
planning, executing object-centred movements
x
-/hOc3d,7P/7
self-motion
object distance
dynamic condition
pointing-selective
parietal
MT/-/21/-
SOG/hOc41a/19
SPL/7PC,7A,mip,ip1-2/7
iPCS/Pfop,6/6,44/6aα inf
FEF/6/6/6aα sup
dorsal attention
externalized attention
visuospatial planning task
aIPL/PFm,PFcm,PFt,Pga/40
daCC/-/32,33
aINS/Ig1-2,Id2-3/13
dlPFC/-/8,9
msPFC/-/24/aCMA
rlPFC/-/10
MFG(BA6)/6/6/6aβ
MFG(BA9)/-/9
fronto-parietal executive control
planning tasks
counting
planning across domains, coupling with
either the default or dorsal attention network
TPJ/Te2.2,PFm,Pga/22,39,40
STS/Te2.2/22
aTL/Te2.1/38
Pcu/7A,7P/7
piPL/PGp/39
pCC/-/3231
HF/HATA/28,34,35
amPFC/FP1-2/10
dmPFC/-/8,9
vmPFC/op5-7/11,25
SFG/6/6/6aβ,pre SMA
IFG/FO1-6/11,47
default mode
dorsal medial subsystem
mentalizing
theory of mind
comprehension
core
self-referential
moral judgements
medial temporal subsystem
episodic memories
autobiographical
prefrontal lateral
prefrontal medial
-/-/24,32/aCMA
cog, lim
xii
-/-/24,32/pCMA
cog, lim
-/6/6/6aβ
coding object-position
orientation arm & body position
xiv
-/6/6/preSMA
control sensory information
visuo-motoric association
declarative phase motor-learning
xiii
-/6/6/SMA proper
posture
volontary movements
motor sequences
FEF/6/6/6aα sup
visuo-sensomotoric control
arm & leg movements
xv
-/6/6/6aα inf
coding peripersonal space
transformation object position
recognition & imitation
grasping movements
-/4p,4a/4
MI
xvi
-/3a,3b,one,2/3,1,2
SI
xvii
-/5l,5m,5mb/5
SII

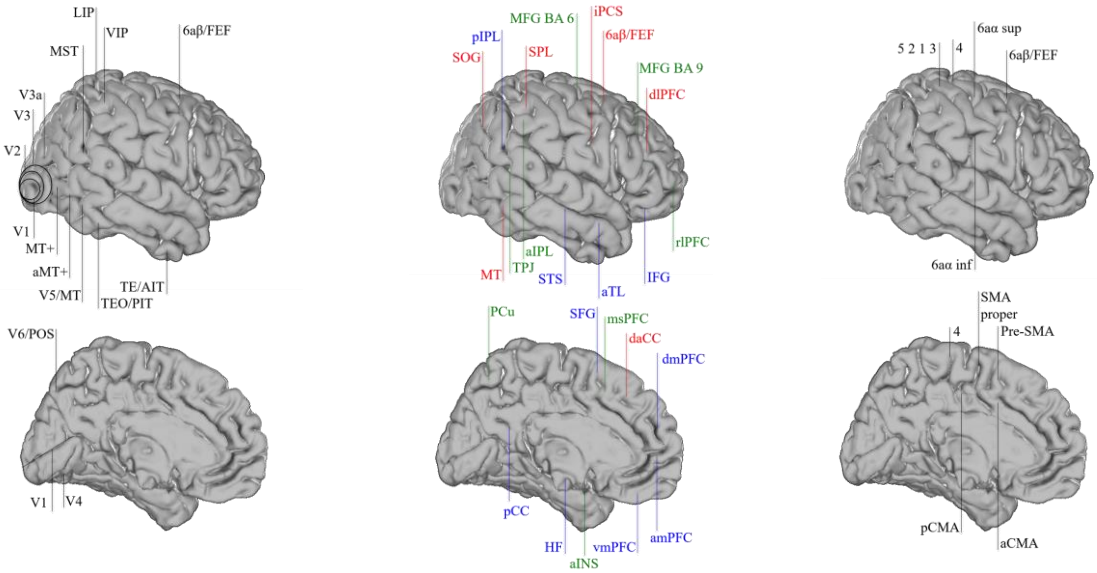
LIP
VIP
6aβ/FEF
MST
V3a
V3
V2
V1
MT+
aMT+
V5/MT
TE/AIT
TEO/PIT
V6/POS
V1
V4
MFG BA 6
iPCS
pIPL
6aβ/FEF
SOG
SPL
MFG BA 9
dlPFC
rlPFC
aIPL
TPJ
MT
STS
aTL
IFG
PCu
SFG
msPFC
daCC
dmPFC
pCC
HF
vmPFC
amPFC
aINS
6aα sup
5 2 1 3
4
6aβ/FEF
6aα inf
SMA proper
4
Pre-SMA
pCMA
aCMA

Tble II. Hierarchies of a visuo-motor task as a temporal linear sequence with nodes and edges from above to bottom:
Upper section of the sequence – the ventral and dorsal visual stream in van Essen's[31] and Ungerleider's[32] adaption and continued development through the synopses of Naser[34], Grandinetti[35], Pitzalis & al.[36] (areas V6, V6A) and Glerean & al.[33]. The ventral stream flows deep into the temporal pole and the dorsal visual stream extends upwards into the parietal lobe over the hierarchies from V1 to V6 and beyond. Yeo & al.[37] consolidate sequential hierarchies within the visual stream along V1 – V3A – MT+ – SPL/7A – FEF using seedbased ICA. Corresponding anatomical sketch bottom left.

Middle section of the sequence – the cognitive networks *default mode* (blue box), *executive control* (green box) and *dorsal attention* (red box) are assigned between visual source and motor output. The executive control network is positioned between default mode and attention[51]. A hierarchical (rostro-caudal and caudal-rostral) order also exists within the prefrontal networks[48] as indicated with the succession of Spreng & al.'s[51] nodes within the respective network boxes. Corresponding anatomical sketch bottom middle, colour of nodes following the colour of the three boxes.

Lower section of the sequence – the output of a visuo-motor task, as per Zille & al.'s[38] and Förstl & al.'s synopsis[67], in a movement and its autoperception. Corresponding anatomical sketch bottom right.

The boxes represent nodes while the connecting edges (black lines) show anatomical adjacency. BA 5 belongs to the upper parietal lobe. There is a local feedback loop present here at least.
Boxes: left column - localisations as per Spreng & al.[51]/Mohlhoff & al.[67]/Brodmann[16]/Zilles & al.[38] and Förstl & al.[67]. Right column - functions.
The coloured column to the right indicates the hierarchical levels following Mesulam[2] (fig. I).

i - *The ventral stream of the human extrastriate visual cortex shows a considerable functional heterogeneity from early visual processing (posterior) to higher, domain-specific processing (anterior)[68]*. This stream comprises an ascending hierarchy with the sequence VI – V2 (V3) – V4 – inferior temporal cortex (IT), *starting with simpler features posteriorly (TEO/PIT) that increase in complexity as processing moves anteriorly (TE/AIT) to perform object recognition*[69]. This stream appears asymmetrical, tending to the right hemisphere[70].
ii - 17[71], V1, primary visual, retinotopic two-dimensional picturing of the external world.
iii - 18[71], gyrus lingualis, occipitalis inferior, V2, spatial filtering, edge detection.
iv - hOc3v[72], lingual cortex, VP/V3v and V4/V4v, construction of a visual space and embedded objects.
v - FG1/FG2[68], fusiform cortex, V4, orientation selective cells concerned with form, and direction selective cells concerned with motion. *The fusiform gyrus hosts several "high-level" functional areas. It is involved in a core network subserving different cognitive tasks, that is, object recognition, visual language perception, or visual attention. It processes high-level visual information associated with faces, limbs, words, and places. FG2 is even a higher-order one*[73].
vi - BA 21, medial temporal gyrus, MT, V5, *it has been connected with processes as different as contemplating distance, recognition of known faces, and accessing word meaning while reading*[74].

vii - The dorsal stream comprises the sequence V1 – V2 (V3) – middle temporal cortex, MT, V5, always retinotopic – medial superior temporal cortex, MST – and finally *intermediate object representations used by the decision-making circuitry further down the dorsal stream in lateral intraparietal sulcus, LIP*[75].
viii - hOc3d[76], cuneus, V3, V3A.
ix - hOc5[77,78], temporo-occipito-parietal TOP-junction, integration of auditory, tactile and visual spaces, V5, MST, related to the deficit symptom of neglect[79].
x - *There is evidence to suggest that there is integration of both dorsal and ventral stream information into motion computation processes, giving rise to intermediate object representations, which facilitate object selection and decision-making mechanisms*[80]. *The areas within the intraparietal sulcus, IPS, in particular, serve as interfaces between the perceptive and motor systems for controlling arm and eye movements in space*[81]. This region is functionally and histologically complex in so as far as several association areas, default mode, executive control and dorsal attention[82,83] overlap in here as well as the cyto-architectonic areas 7A, 7PC, mip, Ip1, Ip2, PF and PFm, sulcus intraparietalis, *concerned with the integration of multimodal information for constructing a spatial representation of the external world in relation to the body or parts thereof, and planning and executing object-centered movements*[83], is processed in V6 and conveyed to V6A for evaluating object distance in a dynamic condition, so to orchestrate the eye and arm movements necessary to reach out.
xi - 7P[84], precuneus, integration to a complex space out of proprioceptive and visual sources, V6, *information on objects in depth which are translating in space, because of the self-motion, is conveyed to V6A, evaluating object distance in a dynamic condition (as that created by self-motion) to orchestrate the eye and arm movements necessary to reach or avoid static and moving objects in the environment*[84], self-perception[85]. *Premotor area engaged in the mental operation, the precuneus aids monitoring the operation in terms of internally represented visual images. Interfaces between the perceptive and motor systems for controlling arm and eye movements in space. Visuomotor tasks comprising target selections for arm and eye movements, object manipulation and visuospatial attention, deficit syndrome of apraxia, neglect, Bálint's syndrome*[86].

xii - aCMA, cingulum anterior, *its proposed role in cognition and its relationship with the arousal/drive state of the organism placing it in a unique position to translate intentions to actions*[87], and being dedicated to the limbic portion of the cortex.
xiii - 6[88], pre-SMA and SMA proper[89,90], intention to act, generation of readiness potential[91,92,93], *action planning and gesture recognition, the operation of the motor monitoring, namely detecting the mismatch between the actual motor output and intended action goal*[94]. *SMA proper and pre-SMA are active prior to volitional movement or action, as well as the cingulate motor area (CMA). This is now known as 'anterior mid-cingulate cortex (aMCC)'. It has been shown by integrating*

simultaneously acquired EEG and fMRI that SMA and aMCC have strong reciprocal connections that act to sustain each other's activity, and that this interaction is mediated during movement preparation according to the Bereitschaftspotential amplitude[89].

xiv - 6aβ, the supplementary eye field (SEF), which has a special role in high level aspects of saccade control, suxh as complex spatial transformations, learned transformations, and executive cognitive functions[95,96]

xv - 6aα superior, visuo-somatomotor area hosting the frontal eye field (FEF)[97], *which constitutes together with the intra-parietal sulcus (IPS) ... an important role in the control of visual attention and eye movements*[81], the coding of object positions[33].

xvi - 4p[98], central sulcus, primary area, *involved in kinematic and dynamic parameters of voluntary movements*[76].

xvii - 3a/3b/one[99], primary area.

xviii - 2[100], the projection emphasising size and shape, secondary unimodal.

xix - 5[101], tertiary, multimodal.

SOG - superior occipital gyrus.
MT - middle temporal; MT+ - medial temporal area; MST - medial superior temporal area; iT - inferior temporal area; PIT - posterior iT; AIT - anterior iT; STS - superior temporal sulcus; aTL - anterior temporal lobe; TPJ - temporoparietal junction.
Pcu - precuneus; piPL - posterioinferior parietal lobe; SPL - superior parietal lobule; alPL - anterior inferior parietal lobule; POS - parietooccipital sulcus; VIP/LIP – ventral/lateral intraparietal sulcus.
HF - hippocampal formation; aINS – anterior insula; pCC - posterior cingular cortex; daCC - dorsal anterior cingulate cortex; CMA – cingular motor area; aCMA - anterior CMA; pCMA posterior CMA.
PFC - prefrontal cortex; rlPFC - rostrolateral PFC; dlPFC - dorsolateral PFC; MFG(BA6) - middle frontal gyrus BA6; MFG(BA9) - middle frontal gyrus BA9; FEF - frontal eye field; mPFC - medial PFC; vmPFC - ventral mPFC; amPFC - anterior mPFC; dmPFC – dorsal mPFC; msPFC - medial superior PFC; SFG - superior frontal gyrus; IFG - inferior frontal gyrus; iPCS - inferior precentral sulcus.

---

feedforward-feedback-loops, we can expect to see interferences appear over longer time and space periods as static or moving waves, described by Crick & Koch[102] as

> *... a forward-traveling, ... propagating net-wave of neuronal activity, (but is not the same as a wave in a continuous medium) ... These net-waves represent at each point in time 'coalitions' ... There are coalitions, which achieve winning status and hence produce [a] conscious experience ... In the conscious mode, it seems likely that the flow is in both directions so that it resembles more of a standing net-wave.*

Its physical nodes (such as location, volume, phase, frequency, amplitude) and edge parameters (such as duration, direction, distance, hierarchy, functions) should be capable of being determined both separately and as arrays.

METHODS

The paradigm[103,104,105] required a visual signal which prompted a test subject to push a button using either their left or right hand following a period they felt was "up to around 15 seconds", with this process monitored using an fMRI scan:

Ten subjects (age range from 21 to 59 years, average age 30 years, 4 female, 6 male, all right-handers, as determined by the Edinburgh Inventory of Handedness) were studied. Informed written consents and approvals by the local ethic commission were obtained. The subjects held a button in each hand and watched visual stimuli presented from a video beamer onto a screen. The stimuli consisted of a short white flash (150 ms) on a black screen, followed by the appearance of a white arrow, which pointed in a pseudo-randomized sequence either to the right, or to the left. The arrow remained visible over the whole trial. The subjects were instructed to press the button with the corresponding thumb (left or right). They were furthermore instructed to choose, for each button press, varying temporal delays from zero up to approximately 15 seconds following the instruction flash. The whole experiment required 20 minutes, during which 87 trials of this delayed response task were presented with pseudo-randomized interstimulus-intervals of 14 +/- 2.5 seconds. The delayed task was contrasted with a speeded response task.

Event-related functional Magnetic Resonance Imaging was performed with a 1.5 Tesla MRI scanner (Siemens Vision, Erlangen, Germany). Twenty-four axial slices with 5 mm thickness and 3x3 mm² in-plane resolution, 64² matrix, 8/8 192 mm² FOV covering the whole brain were acquired using a gradient recalled single shot echo-planar-imaging sequence. To shorten examination time TE was set to 40 ms. The measurement time for one whole brain acquisition was 2.32 seconds and volume repetition time was 2.52 seconds. Thus, for each experiment, 480

whole brain measurements were performed during a time interval of 20 minutes resulting in a mean of 5.5 volume measurements for each trial.

The image evaluation was performed with the Statistical Parametric Mapping programme package (SPM99, Wellcome Department of Cognitive Neurology, London). Preprocessing of the single subject time series images consisted of i) slice-timing, referring to the first slice (top), ii) realignment with sinc interpolation and adjusting for sampling errors, iii) non-linear normalisation to the canonical echo planar target image in Montreal Neurological Imaging space, interpolated with 2 x 2 x 2 mm^3 voxel size, in order to achieve maximal spatial signal-resolution in the group statistics, and iv) spatial smoothing with a Gaussian filter with full-width half-maximum of 6 mm.

To generate time-resolved statistical maps, a series of models was calculated with time-shifted event delays. For each delay, the BOLD response was modelled using a generic hrf (global scaling, specified high-frequency-filter, using the hrf as low-pass-filter, which corresponds to a Gaussian filter with a cut-off level of 4 seconds full-width half-maximum, and without correcting for further internal correlation), resulting in separate t-maps for time points prior to the signal and the self-paced movements (-2 s for the signal, -3.5 s for the movements) and following (6 s for the signal, 2.5 s for movements). T-values were scaled for each volume proportionately from threshold ($p < 0.001$) to individual volumes extreme t-value at point in time t_e. The resulting values were assigned to a baseline corrected[106] activity I. Spatial segmentation used the algorithm of Tzourio-Mazoyer, leaving only regions which excised 10% volume activity, except figure III, insert i.

RESULTS

The resulting phase images of the visual and both motor time series are shown in figure II (respective, detailed time series are given in the supplementary, figures SI & SII, accentuated in a cinematic representation in the supplementary, mov. II). Already the visual inspection gives well separated clusters in a broad macroscale spatio-temporally gradient in figure II:

Two clusters are found in the visual branch (fig. II, left insert red-brown) which correspond to the primary occipital and secondary visual level of association; as well as a further two clusters (fig. II, left insert green-blue) which correspond to the heteromodal parietal and medial supplementary motor level of association. This latter intimate connectivity has not been described to date.
The medial supplementary motor cluster recurs (fig. II, right inserts blue-green) in the motor branch and a second lateral primary/secondary/tertiary sensorimotor cluster (fig. II, right inserts green-red) appears.

The individual false colours represent layers according to Hebbian[1] principles. The false colours red/brown and green/blue illustrate dynamic networks. The clusters develop temporally with wave fronts covering expansive hierarchical, dynamic-functional, anatomical, cyto- and myeloarchitectonical and functional areas, parallel and perpendicular, quantified in table III:

i) Hierarchical architecture (fig. III, insert i & ii) shows the phenomenon of a linear *traveling netwave* over the visual perception, discrimination and higher association levels as delinated by Mesulam[2,3]. This demonstrates the starting point in early idiotypical, primary areas and its evolution over time via secondary unimodal to multimodal high association areas, located midparietal. These midparietal regions high-association areas are omitted in a speeded response task, demonstrating their high hierarchical position (fig. III, insert ii).
The reversed hierarchy is present in the movement-linked development from limbic regions over secondary to primary unimodal motor back to secondary unimodal somatosensory and tertiary heteromodal areas.
Over the course of time the process recruits all the four Mesulam hierarchies over nine nodes (tab. III, col. 1, compare to tab. II, right col.).

ii) DfMRI in its temporal architecture is obvious in a sequence over seven networks with sixteen nodes, representing their hypothesized functional succession (tab. III, col. 2):
At first, consecutive visual networks[36,37,40,42,45,47,54-56], as identified by Smith & al.[40] – the occipital, lateral and medial visual network, with the latter two forming the high-level visual network, as per Zhang & al.[54] – begin to develop, replicating and even refining Yeo[37]'s visual hierarchies.

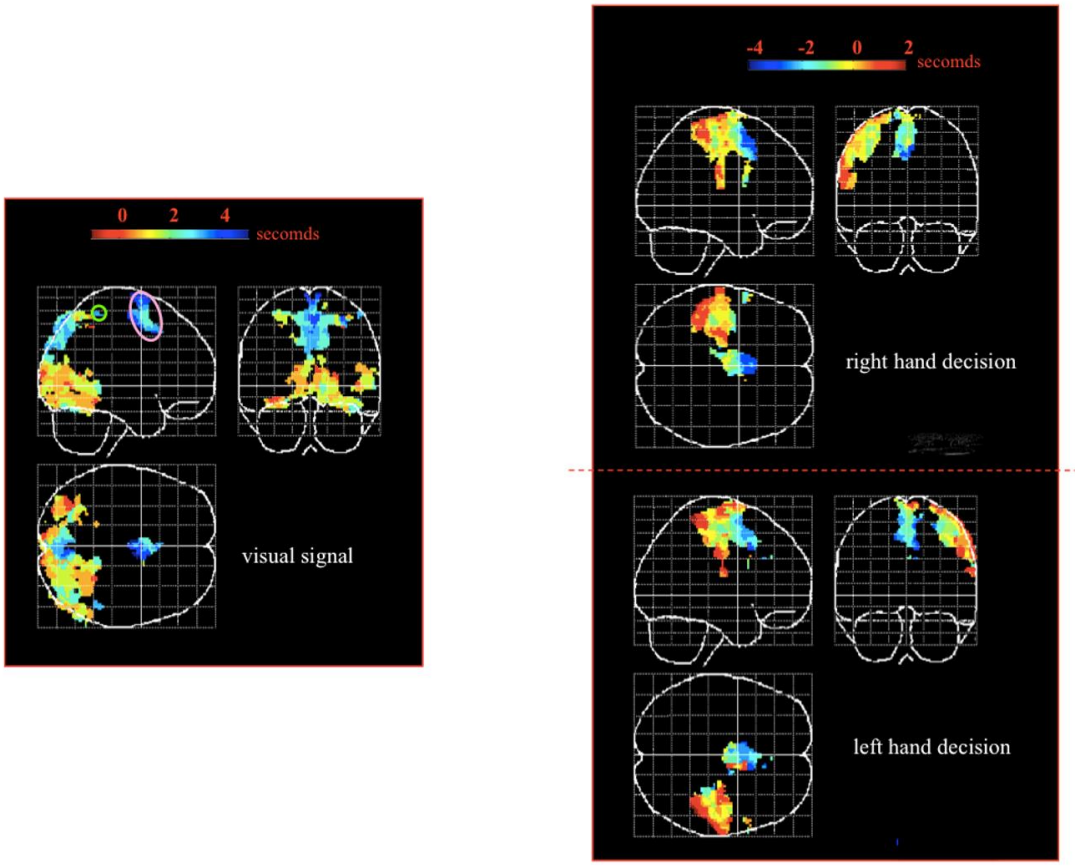

Figure II. Phase images of a self-triggered response task.
Phase of amplitudes of the time series (sup. mov. II, figs. SI and SII) shows the process of an optically triggered, imperative, self-delayed response task.
Maximal-intensity-projections of the point-in-time of extreme activities as indicated by the colour bars. Left image event-related to the signal, and the two right pictures event-related to the respective reactions; stimulus-related from 1 second pre-stimulus (red) to 4 seconds post-stimulus (blue); reaction-related from 4 seconds prior to the reaction (blue) to 2 seconds after the reaction (red). The same colour bar codes hierarchies, separating unimodal (red/brown/green) from heteromodal (green/blue) areas.
Note the spatio-temporal gradient spanning from the calcarine sulcus over the medial, lateral and inferior extrastriate cortex to the precuneus and superior parietal cortex, and from the deep mid-frontal pre-SMA to the upper SMA proper (purple circle), where the same spatio-temporal gradient starts in the motor images, followed within the lateral convexity by gradients from the central sulcus to anterior and to posterior areas, 7PC/mip (green circle) extending up to the latter visual superior parietal side.

The dorsal attention network[37,45,47,48,51,54-57], including Spreng[51]'s nodes MT, SOG, SPL, FEF and daCC (see tab. II), follows parietal and ultimately the medial-precentral part of the sensory motor network[55] originates with the latter.
This and the anterior cingulate cortex, a part of the ventral attention[45,62,63] network is also the origin of the motor branch which subsequently employs the ventral motor network[54], and flows posteriorly and anteriorly into the dorsal attention network and inferiorly towards the Roland's motor operculum in the direction of the insular lobe, spreading in an almost elliptical fashion from the sulcus centralis of the ventral motor network.

iii) Anatomical network architecture (tab. III, col. 3-6) quantifies the datasets with AAL for large anatomical regions in even more temporal details, over even 15 nodes. The quantification gives activated volumes (tab. III, col. 4; approx. 1/5 of the respective AAL regions, accumulating in total to almost 10000 mm^3 in each hemisphere; with an outer layer thickness[107] of 2.3 - 2.8 mm, a neural coverage of 0.25 x 4 x 10 cm^3 for a surface[108] of 1200 cm^2). Identifying first, extreme (tab. III, col. 5) and last point in time of correlation allows modelling of the regional *standing netwaves*[102]. This results in phase-shifted waves as though in conformity with classic wave equations, the frequencies moving in the delta band (tab. III, col. 6), which develop as *standing netwaves*

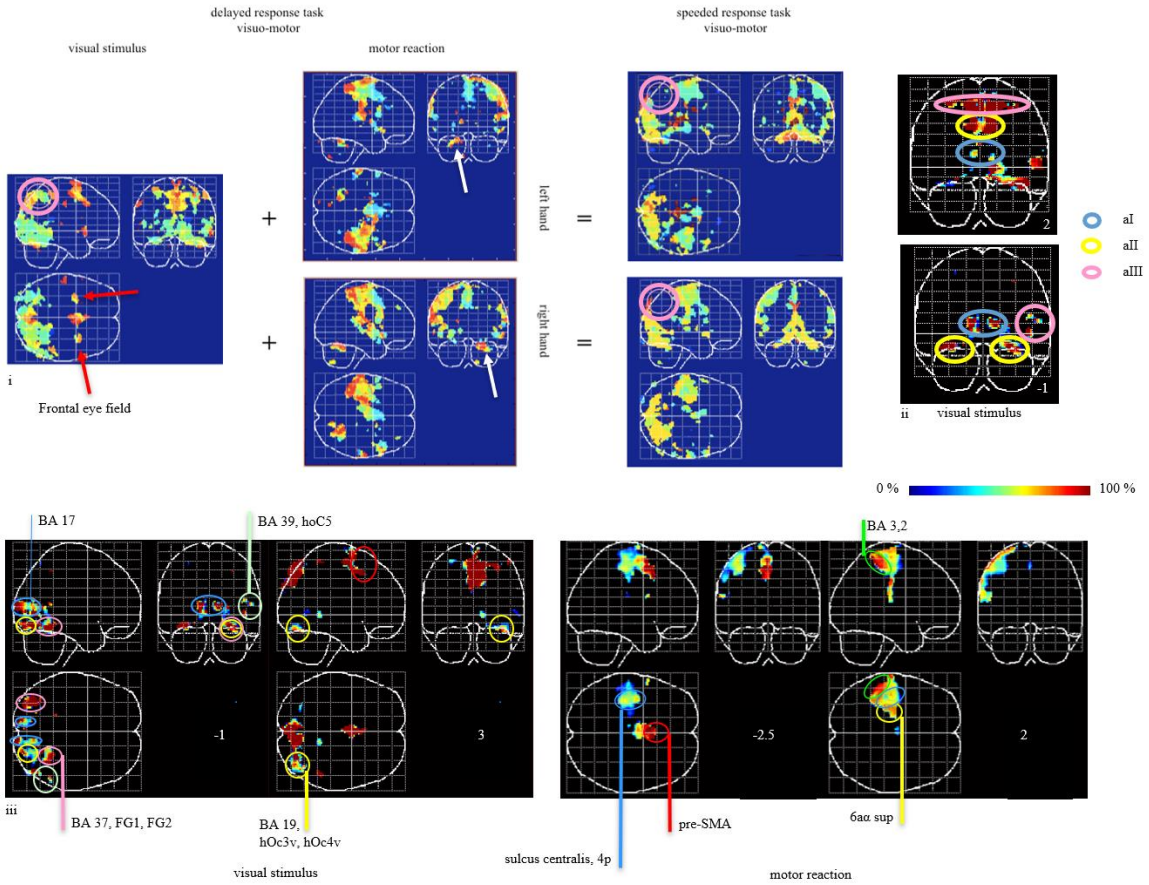

Figure III. Examples of the architecture of a traveling netwave.

i - Contrast of delayed and speeded responses, phase images.
The unique hierarchical position of the complex made of the parietal Brodmann area 7, a core area of the dorsal attention network[37,45,47,48,51,54-57], becomes clear in contrast imaging of speeded and delayed-response tasks. The speeded responses (the right-hand phase images) activate all of the same regions as the delayed responses (the visual phase image on the left, next to it both motor phase images) – with the exception of the high-association superior parietal regions (precuneus and parietalis superior, BA 7, pink rings). The high-association areas are apparently used only when they are involved in long-lasting feedforward-feedback-loops or, in short, in the case of accelerated responses, there is no time left for daydreaming.
The asymmetry[70] of the visual stream is retained in the accelerated response. The red arrows indicate the frontal eye field, not found in the segmented images. The white arrows indicate the cerebellum also not present in the segmented images but discussed[103,104] elsewhere,

ii – Mesulam's[2,3] hierarchies at different times (1s pre-signal, 2s post-signal). Blue line – idiotypical (primary) areas aI; yellow line – modality-specific (unimodal) association areas aII; pink line – high-order (heteromodal) association areas aIII (see fig. I). The coloured bar at the bottom symbolises activity.

iii - Cyto- and myeloarchitecture of a traveling netwave as seen in different time windows.
White numbers represent seconds in relation to the event. The coloured bar top-right symbolises activity. Labeling following Jubrain[21] and Brodmann[16,17].
The visual paradigm's results are shown left. The early events (ventral visual stream, the "what"-stream) shown on the right have disappeared on the later, left-hand side while the late events (dorsal visual stream, the "where" stream) on the left-hand side are not visible early on.
The two right pictures give the executive paradigms according to which the same anticorrelation of the hemodynamic response functions occurs for the medio-prefrontal and lateral sensorimotor networks.

signal

dfMRI	AAL	v mm^3	t_{er} s	f Hz	BA	Jubrain	v mm^3	t_{er} s
vp	calcarinus	820	0.1	0.50	17	17	820	0.0
vl	temporal mid.	324	0.5	0.33	21	hOc5	199	0.1
					21	21	125	1.2
vl	fusiformis	1108	0.6	0.25	37	FG1	776	0.1
					37	FG2	272	1.8
vl	lingualis	1334	0.7	0.33	18	18v	856	0.3
					19	hOc3v	468	1.5
					36	36	60	2.1
vm	occipitalis inf.	140	1.1	0.50	19	hOc4v	140	1.1
vm	cuneus	370	2.0	0.25	18	18d	200	1.5
					19	hOc3d	170	2.4
dat	par. sup.	511	2.0	0.20	7	ip1	111	0.5
					7	mip	148	2.0
					7	7PC	52	2.6
					7	7A	200	2.8
dat	precuneus	686	2.8	0.33	7	7P	686	2.8
sm	SMA	356	3.2	0.25	6	pre-SMA	314	3.1
					6	SMA proper	42	3.9

reaction

dfMRI	AAL	v mm^3	t_{er} s	f Hz	BA	Jubrain	v mm^3	t_{er} s
vat	cingulum med.	220	3.0	0.29	32,24	aCMA	220	-2.2
sm	SMA	545	3.8	0.20	6	pre-SMA	320	-2.1
						SMA proper	140	-1.6
						6aβ	259	1.3
sm	precentral	1589	4.3	0.25	6	6aα sup	366	1.6
					4	4p	1223	-1.6
sm	postcentral	2141	5.2	0.25	3,1,2	3a, 3b, eins, 2	1934	0.0
dat					7	7PC	207	1.7
vm	rolandic op.	253	5.3	0.50	43	Pfop/6aα inf	253	1.8
vm	par. inf.	202	5.9	0.29	40	PFt	202	1.9

Table III. Hierarchical, functional, anatomical and histological visuo-motor dynamics for the right hemisphere.
Left table the signal; right table the reaction.
Classification following Mesulam[2,3] (col. 1, the colors following the signification out of fig. I, compare with fig. II); dynamic functional resonance imaging (col. 2, networks: vp – visual primary; vl – visual lateral (ventral stream); vm – visual medial (dorsal stream); dat – dorsal attention; vat – ventral attention; sm – sensorimotor; vm – ventral motor); AAL, automated anatomical labeling[9] (col. 3 - 6); BA – Brodmann[16] areas (col. 7); Jubrain[21] (col. 8) - but the differentiation within the large surface region 18 between 18v (18 ventral, gyrus lingualis) and 18d (18 dorsal, cuneus and gyrus occipitalis); also the as yet in JuBrain uninvestigated Brodmann areas 36 and 21; also aCMA, a small portion of BA 32 and the differentiation of the large surface volume of SMA according to myelographic classification (tab. II, right insert); v - volume in mm^3; t_{er} - the average points in time of maximal correlations for a given node in seconds related to the event; f – frequency; Hz – Hertz.

$$I_r = e^{-(t-t_{er})^2 f}$$

where *r* is the coordinate, its 1 base-normalised regional nodes activity I_r, the time *t*, the mean time point t_{er} of the maximum regional activities, and frequency *f*.

The individual regions develop in parallel as *winning coalitions*[102] and form a *forward traveling netwave*[102] across time and space (sup. tab. SI).

iv) The cytoarchitectonic network resolution augments the number of nodes up to 26 (tab. III, col. 7 - 10). Relationships for two points in time situated very far apart from one another are extracted in figure III (insert iii) from the time series in the supplementary figures SI & SII. The images demonstrate extreme values over time as so that the earlier images show the cytoarchitecture activated at first points in time, whereas the later images show the cytoarchitecture at the end points in time. The first and late points in time are linked by the waves, shown in

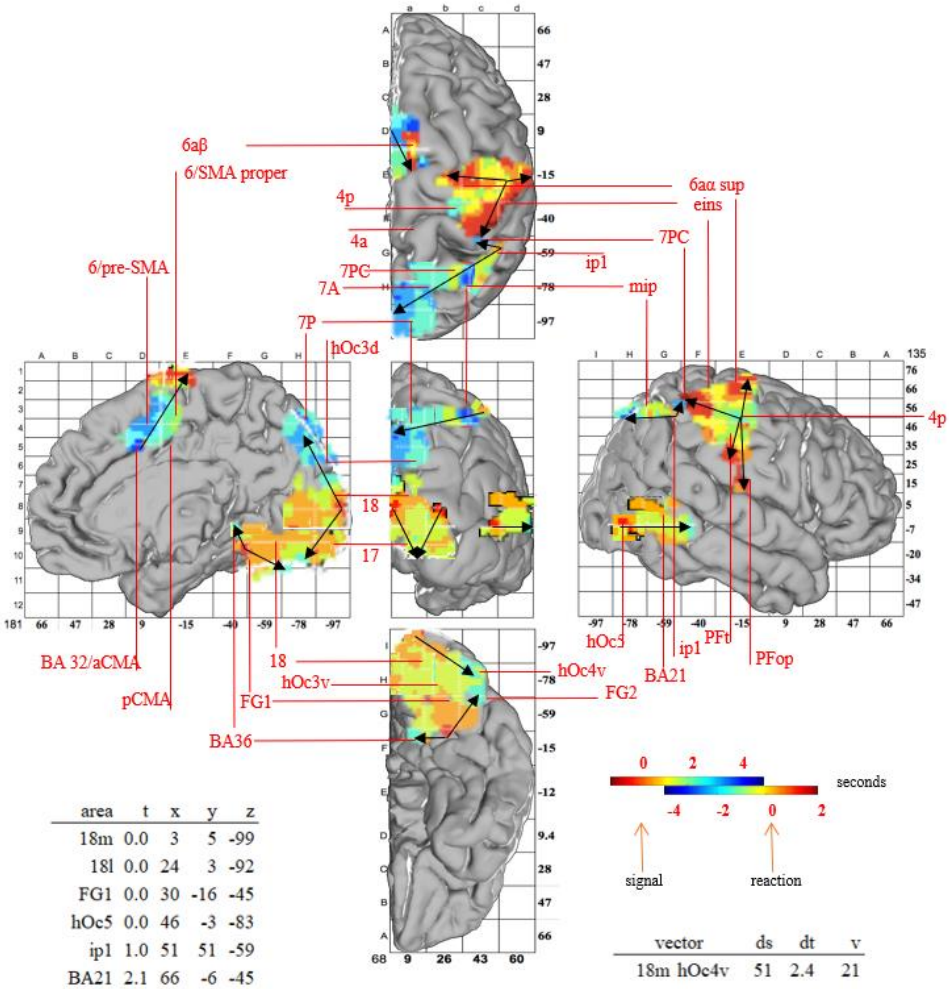

area	t	x	y	z
18m	0.0	3	5	-99
18l	0.0	24	3	-92
FG1	0.0	30	-16	-45
hOc5	0.0	46	-3	-83
ip1	1.0	51	51	-59
BA21	2.1	66	-6	-45
aCMA	2.2	3	31	12
hoC4v	2.4	40	-23	-78
FG2	2.6	42	-27	-68
BA 36	2.7	13	-7	-40
7p	3.0	5	39	-78
7PC`	3.0	43	62	-51
4p	5.2	54	51	-17
6aβ	6.5	12	72	-15
6aα sup	6.7	28	71	-13
Pfop	6.8	68	11	-14
PFt	6.9	66	30	-20
7PC``	7.0	43	62	-48

vector	ds	dt	v
18m hOc4v	51	2.4	21
18m 7P	40	3.0	13
18l hOc4v	34	2.4	14
FG1 FG2	28	2.6	11
FG1 BA36	20	2.7	7
hOc5 BA21	43	2.1	20
ip1 7PC`	16	2.0	8
ip1 7P	51	2.0	26
aCMA 6aβ	62	3.0	21
4p 6aα sup	33	1.5	22
4p PFt	24	1.7	14
4p PFop	42	1.6	27
4p 7PC``	36	1.8	20

Figure IV. Dynamic topology of a visuo-motor vector field.
The right hemisphere from figure III, combined, surface-rendered and the histological architecture as per the definitions of JuBrain[21,66], with the exception of BA 21 and 36, which are not yet published. The subclassification of SMA/BA 6 as per Zilles & al.[38]. 18m – medial (cuneus), 18l - lateral part (gyrus occipitalis) of dorsal JuBrain-area 18.
The colour bars provide the time scale in reference to visual perception and movement in seconds (sup. mov. III).
Both temporal and spatial extreme values were determined within the regions and vectors extrapolated (black arrows).
The table to the left provides the extreme values for space (x, y, z – Talairach[5]-coordinates in mm) and time (t in seconds, the time-arrow of the reaction transposed by -5.2 seconds to visual perception).
The table to the right provides the vectors with their Euclidian distances in time (dt, in seconds) and space (ds, in mm).

figure II. The ventral visual stream is now composed of 17[71], FG1[73], 18v, hOc4v[72], hOc3v, FG2, BA 36, with a midtemporal branch hOc5-21[77-79]. The dorsal ventral stream is composed of 17, 18d, hOc3d[76], ip1[80-83], mip, 7PC, 7A, and 7P and finally, a new observation, BA 6, pre-SMA[88-94]. The corresponding volitional motor response is made of a medial part from aCMA[89] over pre-SMA, SMA proper to 6aβ[38] and a lateral part from 4p[98] to prefrontal 6aα superior[38], as well as to postcentral 3, one, 2[99,100] and further on to 7 pc[79-86], and to caudal PFt, Pfop[78].

DISCUSSION

There is a medio-ventral cluster in the visual branch (fig. III, pink oval). The same cluster is activated in the motor branch through the movement. The clusters overlap over 356 mm^3 and are constructed out of the same microanatomical, functional and temporal elements. Activation begins in pre-SMA (visual 3.1 s post, motor 2.1 s pre) and flows over the SMA proper into 6aβ (visual 3.9 s post, motor 1.3 s post). In the motor branch, there is even a temporally and spatially extended, earlier wave from the aCMA over the same inferior to the same superior medial wall into the medial upper border of the mantle.

A joint time period is therefore consolidated in which a time arrow of 5.2 seconds represents the time from one perception to the reaction, the phase 2π in Mesulam's model (fig. I). In figure IV, using this time arrow a surface projection is carried out for the right hemisphere and the individual histo-architectonical structures.

The temporal and spatial extreme values can be determined within these networks. Via spatio-temporal path minimisations, vectors (black in fig. IV) span a field from the source of the visual perception through the conscious reflexion to the action output into the newly emerging autoperception. Putting it together leads to a vector matrix bridging the combined visual occipito-temporo-parietal-midprefrontal and sensorimotor prefrontal-parietal networks. By way of vectors constructed in this way, a wave develops as Hayne's *stream of consciousness*[109].

Electroencephalography or electrocorticography (ECoG) multichannel recording technologies, with very high spatial (up to 20 micrometres) and temporal (up to 1 millisecond) resolution, capturing power in the 80–150 Hz high-gamma band, have already revealed travelling waves of neural activity as spatiotemporal activity patterns in the cortex in multiple sensory, motor and cognitive systems. *They travel along brain networks at multiple single-area (mesoscopic) and whole-brain (macroscopic) scales, placed as wave generation and propagation in recurrent networks, which may serve a variety of functions, from long-term memory consolidation to processing of dynamic visual stimuli or are even an epiphenomenon.* The resulting ECoG-vectors do not cover the whole process from stimulus to reaction, have propagation speeds from 0.1 to 0.8 metres per second, 5-30 Hz, travelling across several millimetres and 200 ms[110]. The vectors constructed in fig. IV have propagation speeds from 0.02 metres per second, 0.5 Hz, travelling across several centimetres, and adding up to a complete stream of about 50 cm length. The vector orientation however is within the extrastriate cortex and the area 4p[111] the same in ECoG as in the vectors presented here.

Methods to exploit the information encoded in time-varying connectivity in resting-state dynamic fMRI have been developed in recent years in order to reach beyond the static measures of resting fMRI[112,113]. This is an important difference to the task positive paradigm used in this study. While resting state might resemble testing an orchestra preparing for the concert, a task positive brain would be like observing a playing orchestra, where time synchronization will occur as the result of supervised Hebbian learning. Finally it is the task-positive space where we look for orbits and attractors[114].

The biological quality of the results is with respect to i) poor subject and measurement number, ii) poor statistical correction, iii) no correction for effects regarding regionally varying hemodynamic response functions, and iv) no correction for the itself traveling hemodynamic flow, impressive and allows a far reaching interpretation as if representing neuronal activities:

This results in striking and novel precision of the evolution of the dorsal and ventral visual stream, as well as their confluence in the parietal association area, as well as their connectivity with the pre-SMA. The results demonstrate in even striking spatio-temporal resolution the evolution of a premotor activation wave from the deep to the upper midfrontal structures and over the lateral primary sensorimotor areas back to parietal association areas and forward to the frontal eye field, a vector matrix which will be useful for source construction in electroencephalography.

The cognitive demands of the paradigm used here are poor. It is a compelling question as to which vectors will represent the sophisticated reflecting task positive brain, as in chess-playing paradigms, where you would expect even simple vector-sets running along the hierarchical-functional gradients described within the default mode network[41], within the three networks dorsal attention, executive control and default[51] or over the rostral-caudal gradient in the lateral frontal cortex[48].

CONCLUSION

Well evaluated neuro-biological networks are reflected in a linear formation: the temporal order is reproduced i) between the dynamic functional networks visual, dorsal and ventral attention, and sensorimotor; ii) between the anatomical regions contained within these networks; iii) between the Brodmann and Zilles areas also found in these regions; iv) inside these areas and v) via functions and hierarchies.

There are high Granger causalities[115] and efficient connectivity between the clusters via the temporal dimension resulting in causal modelling[116,117] as a suitable process. The phenomenon is formally described by simple cases of the Fokker-Planck dispersion[118]. Geometric waves are observed 'hovering' in the event of high over time synchronisation[119,120] between input and output, in a similar fashion to a taut bow string.
The Crick & Koch's[102] concept of consciousness a *a forward-traveling, propagating net-wave of neuronal activity* holds true and its quantification as phase-shifted synchronisation[121] includes the simplification of biophysical and dynamic causal models[122,123], as well as field theory[118].
The Mesulam and more deeply stacked hierarchical models can be linearly parametrised in task-positive networks accordingly.

Apart from these fundamental aspects it now seems reasonable that the vector-matrix detected here, even regarding the above-mentioned distortions, is strong enough to be inverted[124] by dynamic applications as multi-channel transcranial alternating current stimulation, inducing a virtual reality.

SUPPLEMENTARY

Movie I. Traveling cortical Netwave, hypothesis[125]. https://youtu.be/cQVBLAThJqk
Jubrain[21,22,66] regions aligned over time and neighbourhood from the visual perception to the voluntary motor reaction, and back over the autoperception and heteromodal association, assigned to the cortical hierarchies (coloured box bottom, right) of Mesulam[2,3], right cortical hemisphere.

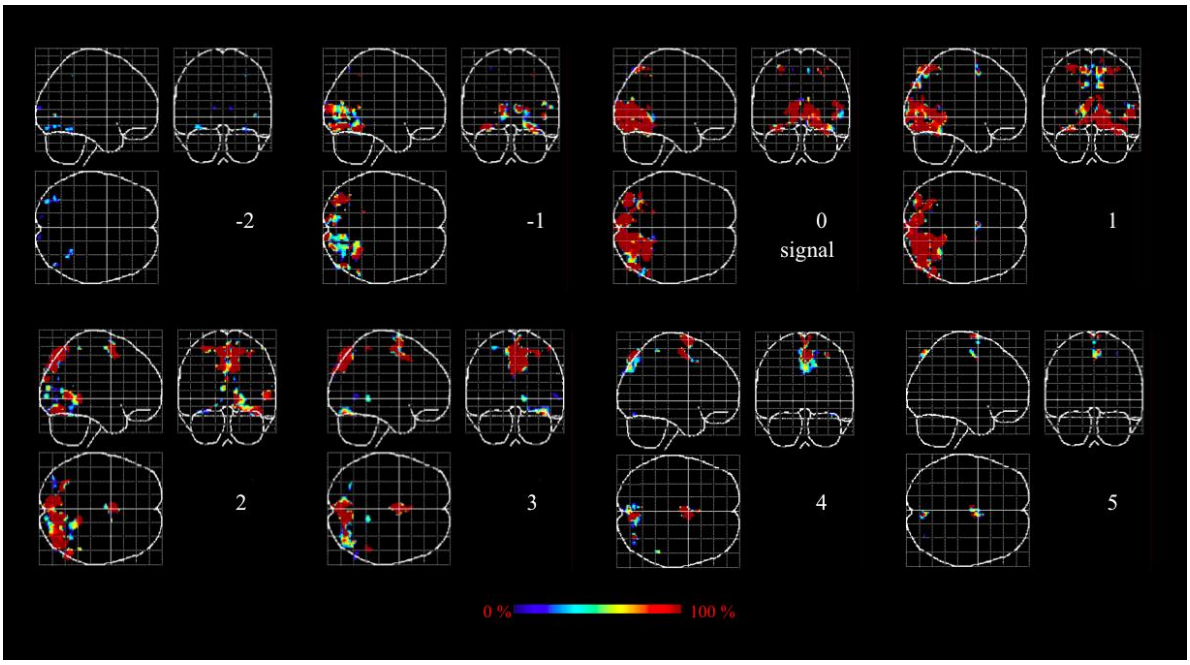

Figure SI. Perception-related time series.
Time steps in second distances (2 seconds ante until 5 seconds post perception, white numbers). Perception at time step three. Activity strength following the colour bar (sup. mov. II, part i).

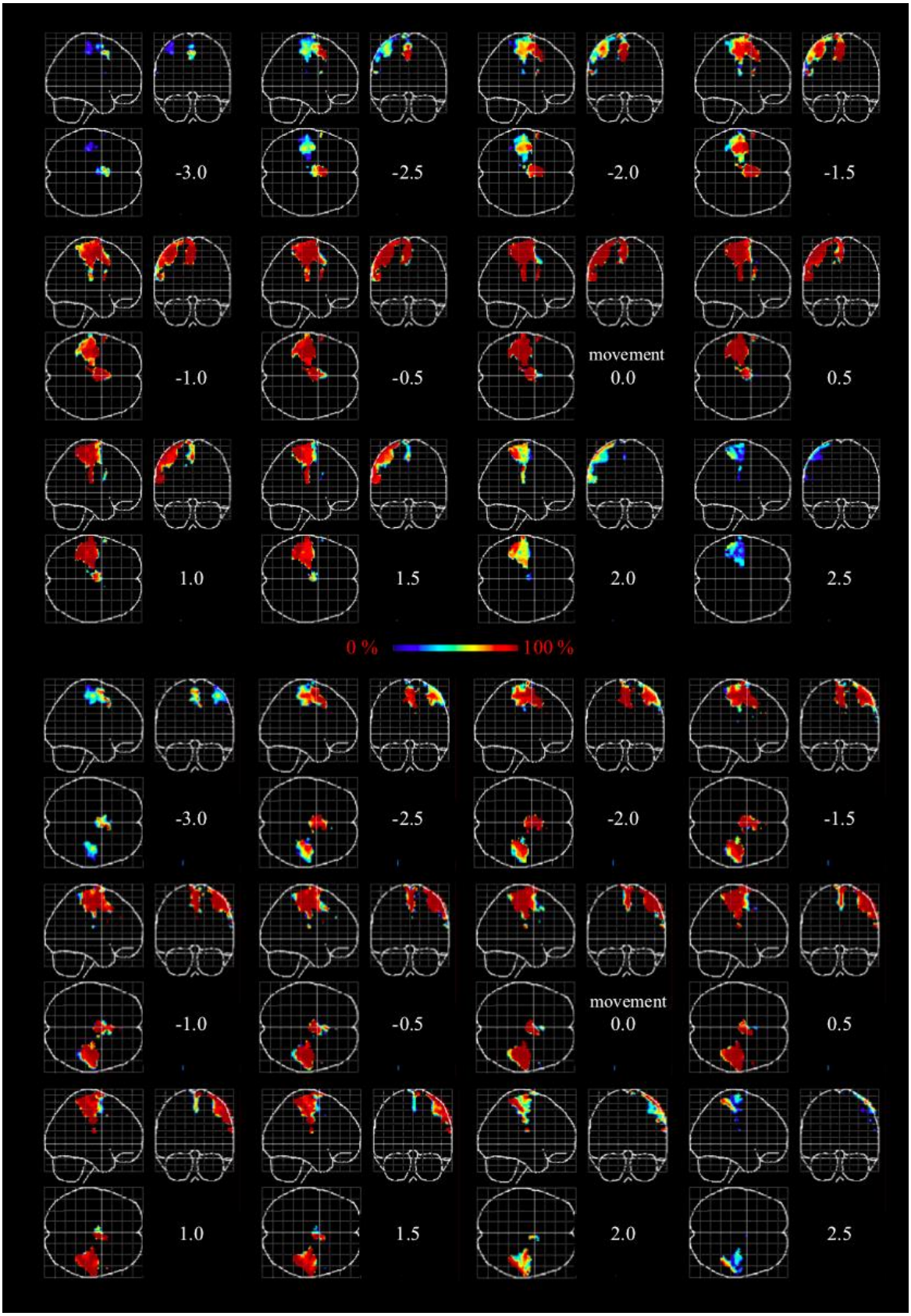

Figure SII. Reaction-related time series.
Right hand - above; left hand - below. Time steps in half second distances (3 seconds ante until 2.5 seconds post reaction, white numbers). Reaction at time step eight. Activity strength following the colour bar (see sup. mov. II, part ii).

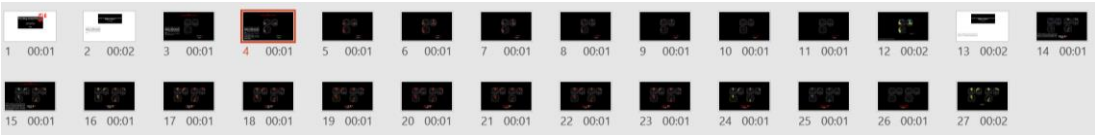

Movie II. Traveling cortical Netwave, results[126]. https://youtu.be/efEaO79gBkM
Part i - The time series for the visual perception, 2 seconds ante until 5 seconds post perception, perception at t = 0 s; last picture the resulting phase image.
Part ii - The right and left hand motor reaction, 3.5 seconds ante until 2 seconds post reaction, movement at t = 0 s; last picture the resulting phase image.
The red-white boxes at the bottom represent the time axis.
Activity strength (scaled t-values of hrf-correlation) following the colour bar at the bottom, but in frame 12 and 27, the resulting phase images, where colour codes time.

AAL	mm³	t mean	f	
	8617			
Parietal_Inf_L	416	5.0	0.3	
Rolandic_Oper_L	317	5.0	0.4	
Postcentral_L	2608	5.0	0.3	
Precentral_L	1657	4.6	0.3	
Temporal_Sup_L	156	4.6	0.3	
Insula_L	158	4.5	0.3	
Heschl_L	15	4.0	1.0	
Cingulum_Mid_L	233	3.8	0.3	
Supp_Motor_Area_L	408	3.0	0.3	right hand
Precuneus_L	353	2.4	0.3	
Cuneus_L	488	1.8	0.3	
Parietal_Sup_L	268	1.2	0.5	
Lingual_L	356	0.4	0.3	
Calcarine_L	745	0.3	0.5	
Fusiform_L	439	-0.2	0.5	visual signal
Calcarine_R	819	0.1	0.5	visual signal
Temporal_Mid_R	324	0.5	0.3	
Fusiform_R	1108	0.6	0.3	
Lingual_R	1334	0.7	0.3	
Occipital_Inf_R	140	1.1	0.5	
Parietal_Inf_R	309	1.5	0.3	
Cuneus_R	370	2.0	0.3	
Parietal_Sup_R	511	2.0	0.2	
Precuneus_R	686	2.8	0.3	
Supp_Motor_Area_R	356	3.2	0.3	left hand
Cingulum_Mid_R	220	3.0	0.3	
Precentral_R	1589	4.3	0.3	
Postcentral_R	2141	5.2	0.3	
Rolandic_Oper_R	253	5.3	0.5	
Parietal_Inf_R	202	5.9	0.3	
	10160			
Supp_Motor_Area_L lha	709	4.0	0.3	
Supp_Motor_Area_R rha	220	4.6	0.3	
Supp_Motor_Area_L rha	1074	4.6	0.2	
Supp_Motor_Area_R lha	877	4.6	0.2	

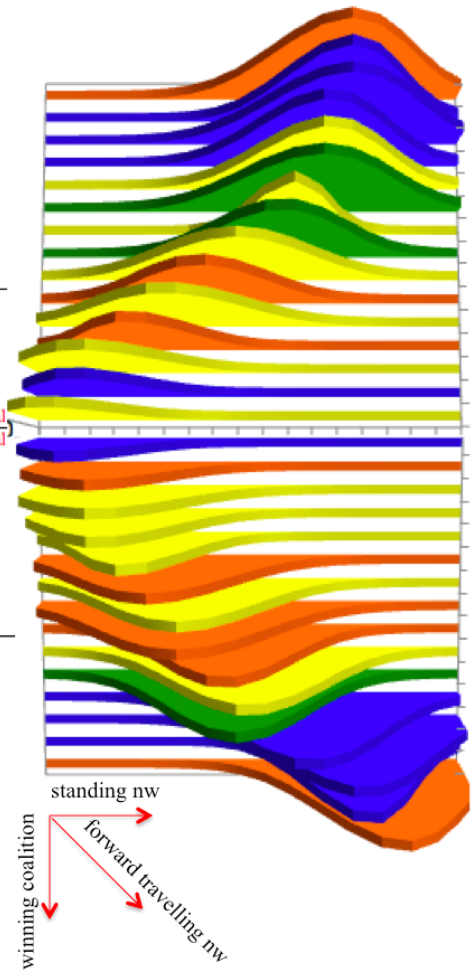

Table IV. Right and left hemisphere in the AAL-network.

Visual event, moving left and right hand; AAL - Anatomical regions following Tzourio-Mazoyer[9]; mm³ –activated volume; t_{mean} – mean-time of maximal activation over all voxels within the region in seconds, relating to and combined with the signal = 0 s (standard deviation 0.5 to 1s); blue numbers for the movement, red for the signal. Black numbers indicate that this region activated under all conditions (the results for the SMA of the visual branch in the table, the results for the other conditions below); f – frequency in Hertz; lha – left hand; rha – right hand; nw – netwave. The colouration of the waves corresponds to Mesulam (fig. I).

Movie III. Traveling cortical Netwave, interpretation[127]. https://youtu.be/fvLWPrw2Ro0
The fMRI time series for the visual perception and the following motor act, fusioned out of movie II for the left hand movement, using the medial supplementary motor area (resulting time axis 2 seconds ante until 8.5 seconds post perception = 7 seconds ante until 2.5 seconds post reaction),
The red-white boxes at the bottom represent the time axis.
Activity strength (scaled t-values of hrf-correlation) following the color bar at the bottom.
The anatomical regions labelled following Jubrain[21,22,66,70-101].
The evolution of different standing netwaves, the resulting travelling netwave and winning coalitions[102] following AAL[9] assigned to the hierarchies of Mesulam[2,3] in the insert above left (see sup. tab. IV).
The red-white boxes at the bottom represent the time axis, scaled in seconds above with respect to the visual signal and below with respect to the motor reaction.
Activity strength (scaled t-values of hrf-correlation) following the colour bar at the bottom, but in frame 19, the resulting phase image, where colour codes time.
Frame 20 gives the surface rendered phase image, right hemisphere, as well as the extreme values in space and time (left table) and the resulting vector-matrix (right table).
Colour codes time, with respect to the signal (upper timescale) and to the reaction (lower timescale).
Labelling JuBrain[2].
Temporo-spatial cortical vectors (black).
Their position in space (x, y, z, Talairach-space (blue boxes) in mm) and time (t in s) as shown in the left table.
Their length in time (dt in s) and space (ds in mm) in the right table.

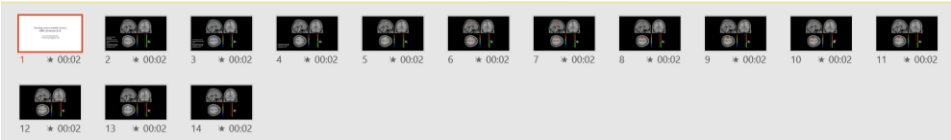

Movie IV. Traveling cortico-cerebellar Netwave[103,128] intended right hand movement, projected on representative anatomical planes. The left colour bar codes activity from blue (low) to red (high). The right colour bar codes time in seconds. Movement at t = 0 s. https://youtu.be/xHpTV9IQJwE

ACKNOWLEGEMENT
This work was supported by the Sektion für experimentelle Kernspinresonanz des Zentralnervensystems der Neuroradiologischen Abteilung der Radiologischen Universitätsklinik der Eberhard Karls Universität Tübingen.
This work was supported by the Henriette Uebersee Stiftung für gefallene Mädchen.

REFERENCES

[1] Hebb D. The Organization of Behavior. *Wiley* New York (1949).

[2] Mesulam MM. From sensation to cognition. *Brain* 121, 1013-1052 (1998).

[3] Mesulam MM. Principles of Behavioral and Cognitive Neurology. *Oxford University Press* (2000).

[4] Deco G. Tononi G. Boly M. Kringelbach ML. Rethinking segregation and integration: contributions of whole-brain modelling. *Nat Rev Neurosci.* 16, 430-439 (2015).

[5] Talairach J. David M. Tournoux P. Atlas d'anatomie stéréotaxique. *Masson* Paris (1957).

[6] Mazziotta JC. Toga AW. Evans AP. Fox A. Lancaster J. A Probablistic Atlas of the Human Brain: Theory and Rationale for Its Development. *Neuroimage* 2, 89-101 (1995).

[7] Ecker A. Die Hirnwindungen des Menschen: nach eigenen Untersuchungen; insbesondere über die Entwicklung derselben beim Fötus und mit Rücksicht auf das Bedürfnis der Ärzte. *Vieweg* Braunschweig (1869).

[8] Smith EG. A new topographical survey of the human cerebral cortex, being an account of the distribution of the anatomically distinct cortical areas and their relationship to the cerebral sulci. *J. Anat.* 41, 237–254 (1907).

[9] Tzourio-Mazoyer N. Landeau B. Papathanassiou D. Crivello F. Etard O. Delcroix N. Mazoyer B. Joliot M. Automated anatomical labeling of activations in SPM using a macroscopic anatomical parcellation of the MNI MRI single-subject brain. Neuroimage 15, 273-289 (2002).

[10] Makris, N. Goldstein JM. Kennedy D. Hodge SM. Caviness VS. Faraone SV. Tsuang MT. Seidman LJ. Decreased volume of left and total anterior insular lobule in schizophrenia. *Schizophr. Res.* 83, 155–171 (2006).

[11] Desikan RS. Ségonne F. Fischl B. Quinn BT. Dickerson BC. Blacker D. Buckner RL. Dale AM. Maguire RP. Hyman BT. Albert MS. Killiany RJ. An automated labeling system for subdividing the human cerebral cortex on MRI scans into gyral based regions of interest. *Neuroimage* 31, 968-980 (2006).

[12] Destrieux C. Fischl B. Dale A. Halgren E. Automatic parcellation of human cortical gyri and sulci using standard anatomical nomenclature. *Neuroimage* 53, 1–15 (2010).

[13] Klein A. Tourville J. 101 labeled brain images and a consistent human cortical labeling protocol. *Frontiers in Neuroscience* 6, 171 (2012).

[14] Auzias G. Coulon O. Brovelli A. MarsAtlas: A cortical parcellation atlas for functional mapping. *Human Brain Mapping* 37, 1573-1592 (2016).

[15] Campbell AW. Histological Studies on the Localisation of Cerebral Function. *Cambridge Univ. Press*, Cambridge, UK (1905).

[16] Brodmann K. Vergleichende Lokalisationslehre der Großhirnrinde in ihren Prinzipien dargestellt auf Grund ihres Zellenbaues. *Barth*, Leipzig (1909).

[17] Lacadie CM. Fulbright RK. Arora J. Constable RT. Papademetris X. Brodmann Areas defined in MNI space using a new Tracing Tool in BioImage Suite. *Human Brain Mapping*, (2008).

[18] von Economo C. Koskinas GN. Die Cytoarchitektonik der Hirnrinde des erwachsenen Menschen. *Springer Verlag* Wien (1925).

[19] Sarkisov SA. Filimonoff IN. Preobrashenskaya NS. Cytoarchitecture of the human cortex cerebri. *Medgiz Moscow* (1949).

[20] Bailey P. von Bonin G. The Isocortex of Man. *Univ. Illinois Press*, Urbana (1951).

[21] Eickhoff SB. Stephan KE. Mohlberg H. Grefkes C. Fink GR. Amunts K. Zilles K. A new SPM toolbox for combining probabilistic cytoarchitectonic maps and functional imaging data. *Neuroimage* 25, 1325–1335 (2005).

[22] Zilles K. Amunts K. Centenary of Brodmann's map. Conception and fate. *Nat Rev Neurosci.* 11, 139-145 (2010).

[23] Vogt C. Vogt O. Allgemeine Ergebnisse unserer Hirnforschung. *J Psychol Neural.* 25, 277-462 (1919).

[24] Flechsig PE. Anatomie des menschlichen Gehirns und Rückenmarks auf myelogenetischer Grundlage, Volume 1. Anatomie des menschlichen Gehirns und Rückenmarks auf myelogenetischer Grundlage. *G. Thieme* (1920).

[25] Geschwind N. Disconnexion syndromes in animals and man. I. *Brain* 88, 237–294 (1965).

[26] Catani M. Ffytch DH. The rises and falls of disconnection syndromes. *Brain* 128, 2224–2239 (2005).

[27] Van Essen DC. Ugurbil K. Auerbach E. Barch D. Behrens TE. Bucholz R. Chang A. Chen L. Corbetta M. Curtiss SW. Della Penna S. Feinberg D. Glasser MF. Harel N. Heath AC. Larson-Prior L. Marcus D. Michalareas G. Moeller S. Oostenveld R. Petersen SE. Prior F. Schlaggar BL. Smith SM. Snyder AZ Xu J. Yacoub E. The Human Connectome Project: a data acquisition perspective. *Neuroimage* 62, 2222-2231 (2012).

[28] Gall FJ. Philosophisch-medizinische Untersuchungen über Natur und Kunst im kranken und gesunden Zustand des Menschen. *Gräffer, Wien* (1791).

[29] Zilles K. Rehkaemper G. Funktionelle Neuroanatomie. *Springer* (1993).

[30] Van Essen DC. Drury HA. Joshi S. Miller MI. Functional and structural mapping of human cerebral cortex: solutions are in the surfaces. *Adv Neurol.* 84, 23-34 (2000).

[31] Van Essen DC. Anderson CH. Felleman DJ. Information processing in the primate visual system: an integrated systems perspective. *Science* 255, 419-423 (1992).

[32] Ungerleider LG. Functional brain imaging studies of cortical mechanisms for memory. *Science* 270, 769-775 (1995).

[33] Glerean E. Salmi J. Lahnakoski JM. Iiro P. Jääskeläinen IP. Mikko Sams M. Functional Magnetic Resonance Imaging Phase Synchronization as a Measure of Dynamic Functional Connectivity. *Brain Connect.* 2, 91–101 (2012).

[34] Naser K. Ricordel V. Le Callet P. in Benois-Pineau J. Le Callet P. Visual content indexing and retrieval with psycho-visual models. *Springer,* 20 (2017).

[35] Grandinetti L. Lippert T. Petkov N. Brain-inspired computing. *Springer,* 53 (2013).

[36] Pitzalis S. Fattori P. Galletti C. The human cortical areas V6 and V6A. *Vis Neurosci.,* 32 (2015).

[37] Yeo BT. Krienen FM. Sepulcre J. Sabuncu MR. Lashkari D. Hollinshead M. Roffman JL. Smoller JW. Zollei L. Polimeni JR. Fischl B. Liu H. Buckner RL. The organization of the human cerebral cortex estimated by intrinsic functional connectivity. *J Neurophysiol.* 106, 1125-1165 (2011).

[38] Zilles K. Schlaug G. Matelli M. Luppino G. Schleicher A. Qü M. Dabringhaus A. Seitz R. Roland PE. Mapping of human and macaque sensorimotor areas by integrating architectonic, transmitter receptor, MRI and PET data. *J Anat.* 187, 515-537 (1995).

[39] Gousias IS. Rueckert D. Heckemann RA. Dyet LE. Boardman JP. Edwards AD. Hammers A. Automatic segmentation of brain MRIs of 2-year-olds into 83 regions of interest. *NeuroImage* 40, 672–684 (2008).

[40] Smith SM. Fox PT. Miller KL. Glahn DC. Fox PM. Mackay CE. Filippini N. Watkins KE. Toro R. Laird AR. Beckmann CF. Correspondence of the brain's functional architecture during activation and rest. *Proc Natl Acad Sci USA.* 106, 13040-13045 (2009).

[41] Andrews-Hanna JR. Smallwood J. Spreng RN. The default network and self-generated thought: component processes, dynamic control, and clinical relevance. *Ann N Y Acad Sci.* 1316, 29-52 (2014).

[42] Andrews-Hanna JR. Reidler JS. Sepulcre J. Poulin R. Buckner RL. Functional-anatomic fractionation of the brain's default network. *Neuron* 65, 550-562 (2010).

[43] Bellec P. Rosa-Neto P. Lyttelton OC. Benali H. Evans AC. Multi- level bootstrap analysis of stable clusters in resting- state fMRI. *NeuroImage* 51, 1126–1139 (2010).

[44] Power JD. Cohen AL. Nelson SM. Wig GS. Barnes KA. Church JA. Vogel AC. Laumann TO. Miezin FM. Schlaggar BL. Petersen SE. Functional network organization of the human brain. *Neuron* 72, 665–678 (2011).

[45] Buckner RL. Krienen FM. Castellanos A. Diaz JC. Yeo BT. The organization of the human cerebellum estimated by intrinsic functional connectivity. *J. Neurophysiol.* 106, 2322–2345 (2011).

[46] Buckner RL. Krienen FM. Yeo BTT. Opportunities and limitations of intrinsic functional connectivity MRI. *Nature Neuroscience* 16, 832–837 (2013).

[47] Choi EY. Yeo BT. Buckner RL. The organization of the human striatum estimated by intrinsic functional connectivity. *J Neurophysiol.* 108, 2242–2263 (2012).

[48] Choi EY. Drayna GK. Badre D. Evidence for a Functional Hierarchy of Association Networks. *J Cogn Neurosci.* 30, 722-736 (2018).

[49] Craddock RC. James GA. Holtzheimer PE. Hu XP. Mayberg HS. A whole brain fMRI atlas generated via spatially constrained spectral clustering. *Human Brain Mapping* 33, 1914–1928 (2012).

[50] Shen X. Tokoglu F. Papademetris X. Constable, RT. Groupewise whole-brain parcellation from resting-state fMRI data for network node identification. *NeuroImage* 82, 403–415 (2013).

[51] Spreng RN. Sepulcre J. Turner GR. Stevens WD, Schacter DL. Intrinsic architecture underlying the relations among the default, dorsal attention, and frontoparietal control networks of the human brain. *J Cogn Neurosci.* 25, 74–86 (2013).

[52] Wang D. Buckner RL. Fox MD. Holt DJ. Holmes AJ. Stoecklein S. Langs G. Pan R. Qian T. Li K. Baker JT. Stufflebeam SM. Wang K. Wang X. Hong B. Liu H. Parcellating cortical functional networks in individuals. *Nat Neurosci.* 18, 1853–1860 (2015).

[53] Joliot M. Jobard G. Naveau M. Delcroix N. Petit L. Zago L. Crivello F. Mellet E. Mazoyer B. Tzourio-Mazoyer N. AICHA: An atlas of intrinsic connectivity of homotopic areas. *Journal of Neuroscience Methods* 254, 46–59 (2015).

[54] Zhang D. Liang B. Wu X. Wang Z. Xu P. Chang S. Liu B. Liu M. Huang R. Directionality of large-scale resting-state brain networks during eyes open and eyes closed conditions. *Front Hum Neurosci.* 9, 81 (2015).

[55] Fan L. Li H. Zhuo J. Zhang Y. Wang J. Chen L. Yang Z. Chu C. Xie S. Laird AR. Fox PT. Eickhoff SB. Yu C. Jiang T. The Human Brainnetome Atlas: A New Brain Atlas Based on Connectional Architecture. *Cerebral Cortex* 26, 3508–3526 (2016).

[56] Gordon EM. Laumann TO. Adeyemo B. Huckins JF. Kelley WM. Petersen SE. Generation and Evaluation of a Cortical Area Parcellation from Resting-State Correlations. *Cerebral Cortex* 26, 288–303 (2016).

[57] Braga RM. Buckner RL. Parallel interdigitated distributed networks within the individual estimated by intrinsic functional connectivity. *Neuron* 95, 457–472 (2017).

[58] Schaefer A. Kong R. Gordon EM, Laumann TO. Zuo XN. Holmes AJ. Eickhoff SB. Yeo BTT. Local-global parcellation of the human cerebral cortex from intrinsic functional connectivity MRI. *Cerebral Cortex* 28, 3095–3114 (2017).

[59] Kong R. Li J. Sun N. Sabuncu MR. Liu H. Schaefer A. Orban C. Zuo XN. Holmes AJ. Eickhoff S. Yeo B.T. Spatial topography of individual-specific cortical networks predicts human cognition, personality and emotion. *Cerebral Cortex* https://doi.org/10.1093/ cercor/bhy123 (2018).

[60] Huth AG. de Heer WA. Griffiths TL. Theunissen FE. Gallant JL. Natural speech reveals the semantic maps that tile human cerebral cortex. *Nature* 532, 453–458 (2016).

[61] Huth AG. Griffiths TL. Theunissen FE. Gallant JL. PrAGMATiC: a probabilistic and generative model of areas tiling the cortex. *arXiv* (2015).

[62] Fan Y. Zeng LL. Shen H. Qin J. Li F. Hu D. Lifespan Development of the Human Brain Revealed by Large-Scale Network Eigen-Entropy. *Entropy* 19, 471 (2017).

[63] Glasser MF. Coalson TS. Robinson EC. Hacker CD. Harwell J. Yacoub E. Ugurbil K. Andersson J. Beckmann CF. Jenkinson M. Smith SM. Van Essen DC. A multi-modal parcellation of human cerebral cortex. *Nature* 536, 171-178 (2016).

[64] Varikuti DP. Genon S. Sotiras A. Schwender H. Hoffstaedter F. Patil KR. Jockwitz C. Caspers S. Moebus S. Amunts K. Davatzikos C. Eickhoff SB. Evaluation of non-negative matrix factorization of grey matter in age prediction. *NeuroImage* 173, 394–410 (2018).

[65] Eickhoff SB. Yeo BTT. Genon S. Imaging-based parcellations of the human brain. *Nat Rev Neurosci.* 19, 672-686 (2018).

[66] Mohlberg H. Eickhoff SB. Schleicher A. Zilles K. Amunts K. A new processing pipeline and release of cytoarchitectonic probabilistic maps – JuBrain. *OHBM Peking, China* (2012).

[67] Förstl H. Hautzinger M. Roth R. Neurobiologie psychischer Störungen. *Springer*, 98-99 (2005).

[68] Caspers J. Zilles K. Amunts K. Laird AR. Fox PT. Eickhoff SB. Functional characterization and differential coactivation patterns of two cytoarchitectonic visual areas on the human posterior fusiform gyrus. *Hum Brain Mapp.* 6, 2754-2767 (2014).

[69] Cowey A. Weiskrantz L. A comparison of the effects of inferotemporal and striate cortex lesions on the visual behaviour of rhesus monkeys. *J Exp Psychol.* 3, 246-253 (1967).

[70] Karnath HO. Insights into the functions of the superior temporal cortex. *Nat Rev Neurosci*. 2, 568-575 (2001).

[71] Amunts K. Malikovic A. Mohlberg H. Schormann T. Zilles K. Brodmann's areas 17 and 18 brought into stereotaxic space-where and how variable? *Neuroimage* 11, 66-84 (2000).

[72] Rottschy C. Eickhoff SB. Schleicher A. Mohlberg H. Kujovic M. Zilles K. Amunts K. Ventral visual cortex in humans: cytoarchitectonic mapping of two extrastriate areas. *Human Brain Mapp.* 28, 1045-1059 (2007).

[73] Lorenz S. Weiner KS. Caspers J. Mohlberg H. Schleicher A. Bludau S. Eickhoff SB. Grill-Spector K. Zilles K. Amunts K.Two New Cytoarchitectonic Areas on the Human Mid-Fusiform Gyrus. *Cerebral Cortex*. 27, 373-385 (2017).

[74] Acheson DJ. Hagoort P. Stimulating the brain's language network: syntactic ambiguity resolution after TMS to the inferior frontal gyrus and middle temporal gyrus. *J Cogn Neurosci.*, 1664–1677 (2013).

[75] van Polanena V. Davarea M. Interactions between dorsal and ventral streams for controlling skilled grasp. *Neuropsychologia* 79, 186–191 (2015).

[76] Kujovic M. Zilles K. Malikovic A. Schleicher A. Mohlberg H. Rottschy C. Eickhoff SB. Amunts K. Cytoarchitectonic mapping of the human dorsal extrastriate cortex. *Brain Struct Funct.* 218, 157-172 (2013).

[77] Malikovic A. Amunts K. Schleicher A, Mohlberg H. Eickhoff SB. Wilms M. Palomero-Gallagher N. Armstrong E. Zilles K. Cytoarchitectonic analysis of the human extrastriate cortex in the region of V5/MT+: a probabilistic, stereotaxic map of area hOc5. *Cereb Cortex* 17, 562-574 (2007).

[78] Caspers S. Eickhoff SB. Geyer S. Scheperjans F. Mohlberg H. Zilles K. Amunts K. The human inferior parietal lobule in stereotaxic space. *Brain Struct Funct.* 212, 481-495 (2008).

[79] Vallar G. Spatial hemineglect in humans. *Trends Cogn Sci.* 2, 87–95 (1998).

[80] Perry CJ. Fallah M. Feature integration and object representations along the dorsal stream visual hierarchy. *Front Comput Neurosci*. 8, 84 (2014).

[81] Grefkes C. Fink GR. The functional organization of the intraparietal sulcus in humans and monkeys. *J Anat.* 207, 3–17 (2005).

[82] Oshio R, Tanaka S, Sadato N, Sokabe M, Hanakawa T, Honda M. Differential effect of double-pulse TMS applied to dorsal premotor cortex and precuneus during internal operation of visuospatial information. *Neuroimage* 49, 1108-1115 (2010).

[83] Kjaer TW. Nowak M. Lou HC. Reflective self-awareness and conscious states: PET evidence for a common midline parietofrontal core. *Neuroimage* 17, 1080–1086 (2002).

[84] Pitzalis S. Fattori P. Galletti C. The human cortical areas V6 and V6A. *Vis Neurosci.* 32 (2015).

[85] Birbaumer N. Sanyung K. Dein Gehirn weiss mehr als Du denkst. *Ullstein*, 230-233 (2016).

[86] Choi HJ. Zilles K. Mohlberg H. Schleicher A. Fink GE. Armstrong E. Amunts K. Cytoarchitectonic identification and probabilistic mapping of two distinct areas within the anterior ventral bank of the human intraparietal sulcus. *J Comp Neurol.* 495, 53–69 (2006).

[87] Paus T. Primate anterior cingulate cortex: Where motor control, drive and cognition interface. *Nat Rev Neurosci*. 2, 417-424 (2001).

[88] Geyer S. Matelli M. Luppino G. Zilles K. Functional neuroanatomy of the primate isocortical motor system *Anat Embryol.* 202, 443-474 (2000).

[89] Nguyen VT. Breakspear M. Cunnington R. Reciprocal interactions of the SMA and cingulate cortex sustain pre-movement activity for voluntary actions. *J Neurosci.* 34, 16397–16407 (2014).

[90] Picard N. PL. Motor areas of the medial wall: a review of their location and functional activation. *Cerebral Cortex* 6, 342-53 (1996).

[91] Libet B. Gleason CA. Wright EW. Pearl DK. Time of conscious intention to act in relation to onset of cerebral activity (readiness-potential). The unconscious initiation of a freely voluntary act. *Brain* 106, 623-842 (1983).

[92] Kornhuber HH. Deecke L. Changes in the brain potential in voluntary movements and passive movements in mean readiness potential and reafferent potentials. *Pflugers Arch Gesamte Physiologie Menschen Tiere*. 284, 1-17 (1965).

[93] Haynes JD. Rees G. Decoding mental states from brain activity in humans. *Nature Reviews Neuroscience* 7, 523-534 (2006). *An assembly of netwaves forms the 'stream of consciousness'.*

[94] Bolognini N. Cognitive processes of motor behavior revealed by tDCS. *Front Neurol.* 8, 29 (2017).

[95] Kirchner H. Barbeau EJ. Thorpe SJ. Régis J. Liégeois-Chauvel C. Ultra-rapid sensory responses in the human frontal eye field region. *Journal of Neuroscience* 29, 7599–7606 (2009).

[96] Graziano MSA. The Intelligent Movement Machine. *Oxford University Press* (2008).

[97] Schall JD. On the role of frontal eye field in guiding attention and saccades. *Vision Research* 44, 1453–1467 (2004).

[98] Geyer S. Ledberg A. Schleicher A. Kinomura S. Schormann T. Bürgel U. Klingberg T. Larsson J. Zilles K. Roland PE. Two different areas within the primary motor cortex of man. *Nature* 382, 805-807 (1996).

[99] Geyer S. Schleicher A. Zilles K. Areas 3a, 3b, and 1 of human primary somatosensory cortex. *Neuroimage* 10, 63-83 (1999).

[100] Grefkes C. Geyer S. Schormann T. Roland P. Zilles K. Human somatosensory area 2: observer-independent cytoarchitectonic mapping, interindividual variability, and population map. *Neuroimage* 14, 617-31 (2001).

[101] Scheperjans F. Eickhoff SB. Hömke L. Mohlberg H. Hermann K. Amunts K. Zilles K. Probabilistic Maps, Morphometry, and Variability of Cytoarchitectonic Areas in the Human Superior Parietal Cortex. *Cereb. Cortex* 18, 2141–2157 (2008).

[102] Crick F. Koch C. A framework of consciousness. *Nat Neurosci*. 6, 119-126 (2003).

[103] Huelsmann E. Erb M. Grodd W. From will to action: sequential cerebellar contributions to voluntary movement. *Neuroimage* 20, 1485-1492 (2003).
Traveling cortico-cerebellar netwave. *Youtube* (2019).

[104] Nolte J. (editor). The Human Brain: An Introduction to its functional Anatomy. *Elsevier*, 510-517 (2008).

[105] Bordier C. Macaluso E. Time-resolved detection of stimulus/task-related networks, via clustering of transient intersubject synchronization. *Hum Brain Mapp.* 36, 3404-3425 (2015).

[106] Cohen MX. Analysing Neural Time Series Data. *The MIT Press* (2014).

[107] Nieuwenhuys R. Donkelaar HJ. Nicholson C. The central nervous system of vertebrates, Volume 1. *Springer*, 2011–2012 (1998).

[108] Toro R. Perron M. Pike B. Richer L. Veillette S. Pausova Z. Paus T. Brain Size and Folding of the Human Cerebral Cortex. *Cerebral Cortex* 18, 2352–2357 (2008).

[109] Haynes JD. Rees G. Decoding mental states from brain activity in humans. *Nature Reviews Neuroscience* 7, 523-534 (2006).

[110] Muller L. Chavane F. Reynolds J. Sejnowski TJ. Cortical travelling waves: mechanisms and computational principle. *Nat Rev Neurosci.*19, 255-268 (2018).

[111] Takahashi K. Saleh M. Penn RD. Hatsopoulos NG. Propagating waves in human motor cortex. *Front Hum Neurosci.* 5, 40 (2011).

[112] Calhoun V. Liégeois R. Time-varying Connectivity in Resting-state fMRI: Methods, interpretations and clinical use. *OHBM* (2019).

[113] Lurie D. Controversies and Open Questions in the Study of "RestingState" Time-Varying Functional Connectivity. *OHBM* (2019).

[114] Breakspear M. Modelling the Multiscale Nature of Dynamic Functional Connectivity. *OHBM* (2019).

[115] Roebroeck A. Formisano E. Goebel R. Mapping directed influence over the brain using Granger causality and fMRI. *Neuroimage* 25, 230-242 (2005).

[116] Friston KJ. Harrison L. Penny WD. Dynamic Causal Modelling**.** *Neuroimage* 19, 1273-1302 (2003).

[117] Friston KJ. Kahan J. Biswal B. Razi A. A DCM for resting state fMRI**.** *Neuroimage* 94, 396-407 (2014).

[118] Deco G. Jirsa VK. Robinson PA. Breakspear M. Friston K. The dynamic brain: from spiking neurons to neural masses and cortical fields. *PLoS Comput Biol.* 4, (2008).

[119] Breakspear M. Terry JR. Friston KJ. Modulation of excitatory synaptic coupling facilitates synchronization and complex dynamics in a biophysical model of neuronal dynamics. *Network* 14, 703-732 (2003).

[120] Erb M. Aersten A. Dynamics of Activity in Biology-Oriented Neural Network Models: Stability at Low Firing Rates. In: Information Processing in the Cortex. Experiment and Theory. Edited by Braitenberg V. & Aertsen A. *Springer* (1992).

[121] Omidvarnia A. Pedersen M. Walz JM. Vaughan DN. Abbott DF. Jackson GD. Dynamic regional phase synchrony (DRePS): An Instantaneous Measure of Local fMRI Connectivity Within Spatially Clustered Brain Areas. *Hum Brain Mapp.* 37, 1970-1985 (2016).

[122] Friston KJ. Ashburner JT. Kiebel SJ. Nichols TE. Penny WD. Statistical Parametric Mapping. *Academic Press* (2008).

[123] Fornito A. Zalesky Z. Bullmore E. Fundamentals of Brain Network Analysis. *Academic Press* (2016).

[124] Fernández-Corazza M. Turovets S. Luu P. Anderson E. Tucker D. Transcranial Electrical Neuromodulation Based on the Reciprocity Principle. *Front. Psychiatry* 27 May (2016).

[125] Hülsmann ERM. Traveling cortical Netwave, hypothesis. *Youtube* (2019).

[126] Hülsmann ERM. Traveling cortical Netwave, results. *Youtube* (2019).

[127] Hülsmann ERM. Traveling cortical Netwave, interpretation. *Youtube* (2019).

[128] Hülsmann ERM. Traveling cortico-cerebellar netwave. *Youtube* (2019).